



RESEARCH ARTICLE SUMMARY

CANCER

Lineage-specific intolerance to oncogenic drivers restricts histological transformation

Eric E. Gardner*, Ethan M. Earlie, Kate Li, Jerin Thomas, Melissa J. Hubisz, Benjamin D. Stein, Chen Zhang, Lewis C. Cantley†, Ashley M. Laughney*, Harold Varmus*

INTRODUCTION: What determines the behavior and appearance of different cancers? Several factors may be involved, including the kind of normal cell from which a cancer arises (the cell of origin) and the set of specific genes (especially tumor suppressors and proto-oncogenes) that are altered during the conversion of a normal cell to a malignant one. The variations in appearance and behavior and the affected genes often correlate with a specific cell of origin, suggesting that different cell lineages show different responses to various genetic changes. Context is key—not every oncogene is broadly oncogenic.

Some types of cancers, such as adenocarcinomas of the lung and the prostate, undergo dramatic changes in appearance and behavior and display an altered genetic profile when they develop resistance to targeted therapies. In lung cancers, this histological transformation (HT) can result in the conversion of lung adenocarcinoma (LUAD) into an aggressive type of neuro-

endocrine cancer indistinguishable from small cell lung cancer (SCLC), which is therapeutically recalcitrant and connotes poor prognosis. These events are considered off-target mechanisms of resistance because the original oncogenic driver pathway is thought to be no longer critical for tumor cell proliferation. Thus, a distinct, separate driver program has emerged.

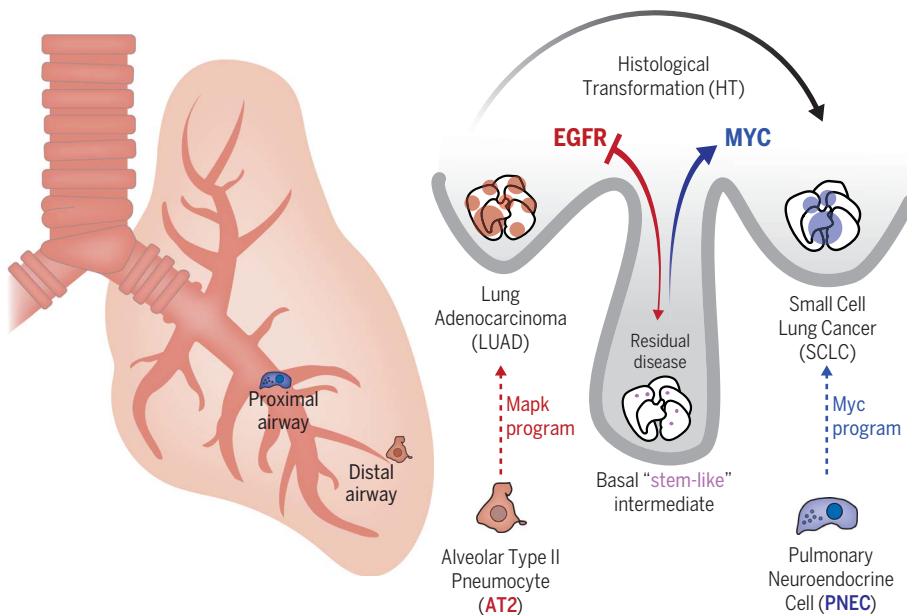
RATIONALE: The complex process of HT is difficult to characterize rigorously in human subjects. But the possibility of modeling HT in the lungs of experimental mice offers an opportunity to study the relationships among cancer phenotypes, cells of origin, and genetic alterations. To that end, we proposed to use genetic engineering to mimic the events observed in human lung HT. We planned to generate LUAD driven by a mutationally activated epidermal growth factor receptor (EGFR) gene and then to transform those tumors into SCLCs by block-

ing the function of the mutant EGFR gene by introducing changes in other genes, such as oncogene *Myc* and the tumor suppressors *Rb1* and *Trp53*. We would then be able to study HT in detail by performing single-cell RNA-sequencing during this process.

RESULTS: We were able to reconstruct pulmonary HT in a mouse model. We then characterized the transcriptional programs throughout three stages: during growth of EGFR-driven LUAD; in the limited disease that remained after reduction of oncogenic EGFR; and during the transformation of tumor cells into neuroendocrine SCLC. By following the expression of single oncogenes in different lung-cell lineages, we demonstrated that the process of HT is regulated by the tolerance of different cell types to distinct oncogenic drivers. Thus, whereas most lung cells are resistant to transformation by *Myc*, neuroendocrine cells are highly sensitive to its oncogenic effects; however, their fitness is impaired by mutated EGFR. Conversely, lung alveolar epithelial cells grow excessively in response to mutated EGFR but are impaired by *Myc* alone.

During the process of HT, undifferentiated stem-like cells accumulate, and some become neuroendocrine in character as SCLC emerges. This process appears to require the loss of two tumor suppressor genes, *Trp53* and *Rb1*, that are almost universally inactivated in human SCLC. Furthermore, we found that loss of yet another tumor suppressor gene, *Pten*, allowed *Myc* to transform the AT2 lineage. However, the additional loss of *Rb1* was required for transformation to a neuroendocrine phenotype. These results suggest that both *Myc* and *Rb1* are critical regulators of neuroendocrine HT.

CONCLUSION: By developing this novel experimental model for pulmonary HT, we have recapitulated the complex sequence of events that depends on varied responses of different cell lineages to changes in a few known cancer genes. These findings will enable efforts to study the responses of various cell types to changes in other genes implicated in carcinogenesis and to explore strategies for treating aggressive cancers such as SCLC with agents that target *MYC* for which approved, targeted therapeutics are not yet available. ■



Histological transformation through a stem-like intermediate. Gardner *et al.* developed a genetically engineered mouse model of histological transformation (HT) of EGFR-driven lung adenocarcinoma (LUAD) to small cell lung cancer (SCLC) and closely examined this phenomenon with single-cell RNA-sequencing. They found that the intermediate state between LUAD and SCLC was stem-like and most closely resembled a pulmonary basal cell.

The list of author affiliations is available in the full article online.
*Corresponding author. Email: eeg2001@med.cornell.edu (E.E.G.); ashley.laughney@gmail.com (A.M.L.); varmus@med.cornell.edu (H.V.)

†Present address: Department of Cell Biology and Dana-Farber Cancer Institute, Harvard Medical School, Boston, MA.
Cite this article as E. E. Gardner *et al.*, *Science* 383, eadj1415 (2024). DOI: 10.1126/science.adj1415

S READ THE FULL ARTICLE AT
<https://doi.org/10.1126/science.adj1415>

RESEARCH ARTICLE

CANCER

Lineage-specific intolerance to oncogenic drivers restricts histological transformation

Eric E. Gardner^{1*}, Ethan M. Earlie^{1,2,3}, Kate Li¹, Jerin Thomas¹, Melissa J. Hubisz^{1,2,3,4}, Benjamin D. Stein^{1,5}, Chen Zhang⁶, Lewis C. Cantley^{1,5,†}, Ashley M. Laughney^{1,2,3*}, Harold Varmus^{1*}

Lung adenocarcinoma (LUAD) and small cell lung cancer (SCLC) are thought to originate from different epithelial cell types in the lung. Intriguingly, LUAD can histologically transform into SCLC after treatment with targeted therapies. In this study, we designed models to follow the conversion of LUAD to SCLC and found that the barrier to histological transformation converges on tolerance to Myc, which we implicate as a lineage-specific driver of the pulmonary neuroendocrine cell. Histological transformations are frequently accompanied by activation of the Akt pathway. Manipulating this pathway permitted tolerance to Myc as an oncogenic driver, producing rare, stem-like cells that transcriptionally resemble the pulmonary basal lineage. These findings suggest that histological transformation may require the plasticity inherent to the basal stem cell, enabling tolerance to previously incompatible oncogenic driver programs.

Histological transformation (HT) is a poorly understood process whereby a cancer's initial histology is altered and presents as a new histologic type of cancer. These changes are presumed to be under the selective pressure of an oncogene-targeted therapy. Best described in the context of epidermal growth factor receptor (EGFR) inhibition in lung adenocarcinoma (LUAD) (1–3) and androgen receptor inhibition of prostate adenocarcinoma (4, 5), these transformations most commonly lead to neuroendocrine and/or squamous differentiation (6). Considered an off-target form of acquired resistance, the cancer's proliferative character is no longer dependent on the original oncogenic driver pathway. In the earliest reports of HT, it was unclear whether the recurrent tumors were independent, primary small cell lung cancer (SCLC), subclones selected for under the pressure of targeted therapy, or products of direct conversion of LUAD into SCLC. Supporting evidence for direct conversion relies on the continued presence of a LUAD driver oncogene within a cancer that is histologically SCLC. Such oncogenic mutations in genes that commonly drive the formation of LUADs have rarely been encountered in genome sequencing studies of primary, treatment-naïve SCLC (7, 8). Most posttransformation samples

have shared, clonally related mutations present in the LUAD before undergoing HT; however, protein expression of the LUAD driver is conspicuously absent after transformation (9). Furthermore, loss of the retinoblastoma (RB) tumor suppressor is observed in cases of HT in both lung and prostate cancers (4, 10), and patients with EGFR-driven LUADs harboring inactivation of *TP53* and *RBI* are at an especially high risk for developing SCLC after targeted therapy (1, 11).

Primary LUAD and SCLC are thought to develop from distinct cell types in the lung: the alveolar type II (AT2) cell and the pulmonary neuroendocrine cell (PNEC), respectively. Much is known about surfactant-producing AT2 cells as a cell of origin for LUAD, for which the EGF signaling pathway is an established mitogenic program (12–14). Hence, activating mutations and amplifications of genes that encode proteins in the mitogen-activated protein kinase (MAPK) pathway, including *RAS* and *EGFR*, are common in LUAD (15). By contrast, SCLC is thought to arise predominantly from PNECs (8, 16, 17). PNECs are rare and are found near anatomic branchpoints of the large airway; they function as sentinels for inhaled pathogens and environmental changes, signaling to other cells through both electrochemical innervation and secretory function (17–19). Because of their scarcity, much less is known about PNEC biology, including what signaling events drive their proliferation.

We hypothesized that the complexity of HT may be simplified to represent a mechanism by which a cell can change its oncogenic driver program. We set out to address several fundamental unknowns: (i) how an adenocarcinoma transforms to a high-grade neuroendocrine cancer, (ii) what the intermediate steps in HT are, and (iii) what the oncogenic driver program of

the pulmonary neuroendocrine lineage is. We addressed these questions by combining models of genetically engineered lung tumorigenesis, lineage tracing, and chronologic single-cell RNA-sequencing (scRNA-seq) to map cell type-specific oncogenic driver programs and their contributions to HT.

Results

Histologically distinct lung tumors in an isogenic mouse model

To chronicle HT, we generated a new genetically engineered mouse model (GEMM) that combines the conditional expression of *Myc*, *rtTA3*, and *tdTomato* (*lox-stop-lox* alleles) with the loss of tumor suppressors *Rb1* and *Trp53* (floxed alleles) and a doxycycline (DOX)-inducible, oncogenic *EGFR* transgene (20). The model (hereafter ERPMT) allows for two classes of manipulations: (i) control of the cell of origin through lineage-restricted expression of Cre recombinase after intratracheal infection by using adenoviral vectors with cell type-specific promoters (21), and (ii) oncogenic *EGFR*^{L858R} expression controlled in a DOX-dependent manner (Fig. 1A). Tumors initiated in the AT2 or PNEC lineages in ERPMT mice produced histologically distinct lung tumors with opposing dependencies on the presence or absence of DOX. If expression of Cre was initiated in the AT2 lineage and the mice received DOX, the ERPMT model developed an aggressive LUAD. By contrast, no mice succumbed to disease in this timeframe if they were off DOX. In mice receiving DOX, we observed multifocal, glandular lesions consistent with LUAD throughout all lobes of the airway, demonstrating homogenous expression of tdTomato (tdTom) and lack of the neuroendocrine marker synaptophysin (Fig. 1B). Conversely, if expression of Cre was initiated in the PNEC lineage, then the cohort off DOX developed an aggressive neuroendocrine SCLC and the mice on DOX appeared healthy at a time when 100% of the cohort off DOX was moribund (Fig. 1C).

LUAD and SCLC tumorigenesis developed with similar penetrance and latency in the ERPMT model. To compare these models transcriptionally, we isolated tdTom⁺ cells in the on-DOX group from the AT2 lineage (hereafter labeled LUAD; red) and the off-DOX group from the PNEC lineage (hereafter labeled SCLC; blue) at 8 weeks on study and performed scRNA-seq. As expected, these tumor cells were transcriptionally distinct and closely resembled their precursors (Fig. 1D and fig. S1, A and B). LUAD cells exhibited mixed AT2 and AT1 character, which is consistent with prior observations in the regenerating airway (22) and in mouse (12) and human tumors (23). Compared with LUAD, SCLC had lower expression of components of the major histocompatibility complex (MHC) class II antigen pathway (fig. S1C), which is consistent with MHC class II deficiency in

¹Meyer Cancer Center, Weill Cornell Medicine, New York, NY.

²Department of Physiology, Biophysics, and Systems Biology, Weill Cornell Medicine, New York, NY.

³Institute for Computational Biomedicine, Weill Cornell Medicine, New York, NY.

⁴Bioinformatics Facility, Institute of Biotechnology, Cornell University, Ithaca, NY.

⁵Department of Medicine, Weill Cornell Medicine, New York, NY.

⁶Department of Pathology and Laboratory Medicine, Weill Cornell Medicine, New York, NY.

*Corresponding author. Email: eeg2001@med.cornell.edu (E.E.G.);

ashley.laughney@gmail.com (A.M.L.); varmus@med.cornell.edu (H.V.)

†Present address: Department of Cell Biology and Dana-Farber Cancer Institute, Harvard Medical School, Boston, MA.

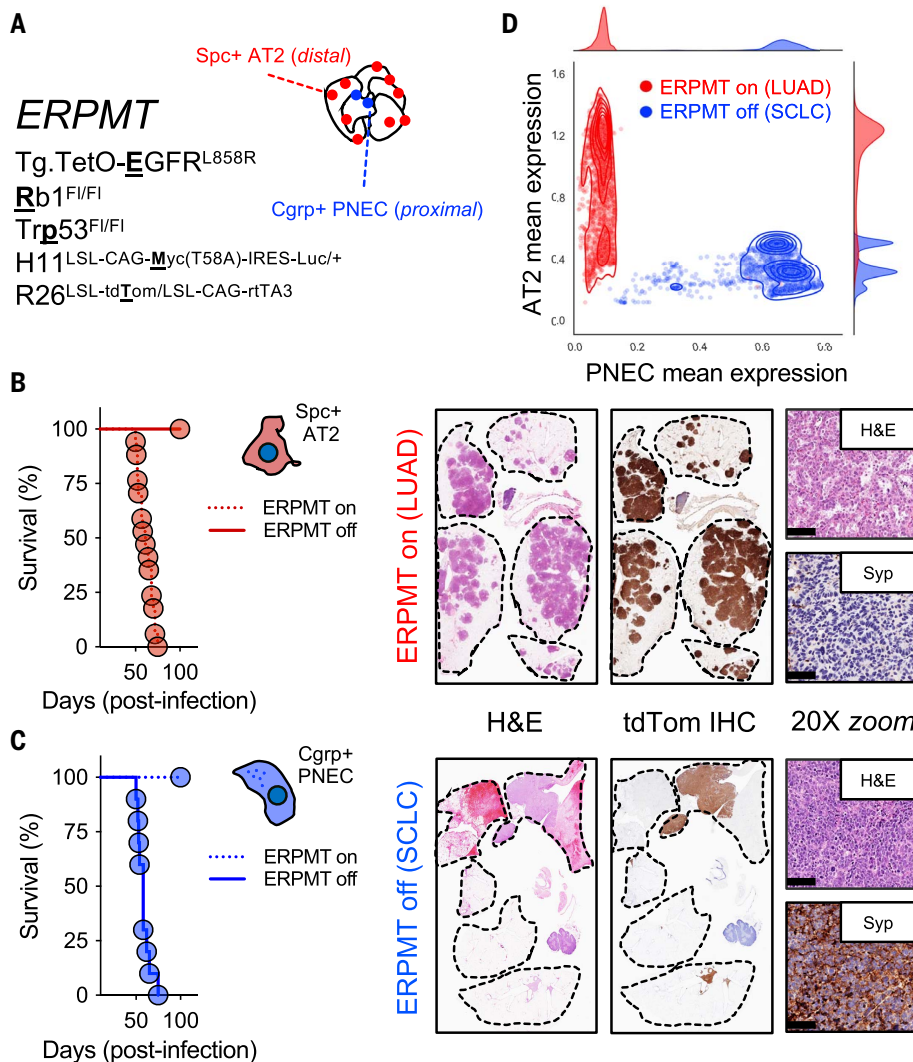


Fig. 1. A GEMM model to generate distinct histologic subtypes of lung cancer. (A) Nomenclature used for the ERPMT model, with abbreviated alleles bolded and underlined and general strategy to use promoter-restricted adenovirus to initiate tumorigenesis in specific airway cells. (B) Survival and histologic appearance of the ERPMT model initiated in alveolar type II (AT2) cells (red cartoon cells) or (C) pulmonary neuroendocrine (PNEC) cells (blue cartoon cells) when mice are on DOX-containing (dashed line; $n = 10$ mice per group) or control diet (solid line; $n = 10$ mice per group). Representative sagittal hematoxylin and eosin (H&E) and tdTomato (tdTom) IHC lung sections alongside high-powered H&E and synaptophysin (Syp) IHC (in boxes on right; scalebars, 100 μm) from the LUAD model initiated from AT2 cells on DOX (above) or the SCLC model initiated from PNEC cells off DOX (below). (D) Mean imputed expression of AT2 and PNEC lineage markers (table S1) in single cells isolated from LUAD (red; $n = 5394$ cells) or SCLC (blue; $n = 4371$ cells) ERPMT models with overlaid kernel density estimates (KDEs) reflecting cell density; tdTom⁺ tumor cells sorted and pooled from $n = 3$ mice at 8 weeks after infection.

primary SCLC (24, 25) and AT2-specific expression of MHC class II molecules (26). Instead, most SCLC tumor cells expressed factors that suppress Notch signaling, including the inhibitory ligand *Dll3* and transcription factor *Hes6* (27). Conversely, the LUAD model was enriched for Notch-stimulating factors, which is in keeping with this model presenting as a nonneuroendocrine, alveolar-derived LUAD (fig. S1D). Additionally, bulk ATAC-sequencing revealed regions of chromatin that mapped to

Notch2, *Hes1*, and *Sftpc* that were differentially accessible in LUAD as compared with SCLC (28, 29). By contrast, the SCLC model had greater accessibility of neuroendocrine genes, including *Insm1*, *Chga*, and *Ascl1* (fig. S1E). Furthermore, differentially accessible peaks in the MAPK-driven LUAD were significantly enriched for activator protein 1 (AP-1) motifs such as *Jun* and *Fos*, whereas several basic helix-loop-helix (bHLH) regulatory elements involved in neurogenesis (*Tcf21*, *Tcf4*, and *Ascl1*) were enriched

in the SCLC model (fig. S1F) (30). Taken together, we generated a mouse model capable of forming two histologically distinct lung cancers that are united by the process of HT—prompting us to ask whether the LUAD tumors in these mice could be encouraged to transform to SCLC.

EGFR removal and the emergence of neuroendocrine character

We speculated that the ERPMT model could be used to understand conversion of LUAD to SCLC, provided adequate selective pressure was applied against the LUAD driver. After the development of late-stage LUAD, we randomized cohorts to one of three arms: remain on DOX (ERPMT on), come off DOX for 1 month and then restart DOX (ERPMT on > off > on), or come off DOX and remain off for the duration of the study (ERPMT on > off). Terminal lung cancers developed at statistically different rates across these perturbations (Fig. 2A). If DOX was permanently removed, the resulting lung tumors were consistent with SCLC, but if DOX was restarted (ERPMT on > off > on), tumors were consistent with LUAD, albeit with fewer, larger lesions than were found in mice continually on DOX (Fig. 2B).

To better understand the proliferative nature of residual disease that emerges upon EGFR withdrawal, we randomized ERPMT mice developing LUAD to come off or stay on DOX after three daily pulses of the S-phase label 5-ethynyl-2'-deoxyuridine (EdU). Three weeks later we labeled again, now with a different S-phase analog, bromodeoxyuridine (BrdU), thus labeling cells with a proliferative history that continued to cycle after tumor regression (fig. S2, A and B). Tumors that remained on DOX were EdU⁺/BrdU⁺, whereas off DOX, residual tdTom⁺ cells were present as single cells and were EdU⁺/BrdU⁻. This result suggested that residual cells did not continue to cycle after DOX removal (fig. S2, C and D).

Manipulating transcription of *EGFR* with DOX is a convenient and effective experimental approach, but it does not precisely recapitulate the clinical scenario in which patients are treated with inhibitors of the EGFR kinase domain. To address this difference, we compared inhibiting the kinase activity of EGFR using osimertinib with the effect of removing DOX, thus gradually extinguishing *EGFR* expression. After 8 weeks of LUAD development, the frequency of tdTom⁺ cells in the airway of ERPMT mice ranged from ~5 to 35%. However, this was reduced to <1% in all animals after 1 month of treatment with osimertinib (osi) (31) or the removal of DOX (Fig. 2C). We isolated tdTom⁺ cells from these groups and found that genetic—as opposed to pharmacologic—suppression of EGFR led to a greater increase in *Ascl1*-expressing cells, the definitive lineage marker of the PNEC (32) (fig. S3, A and B).

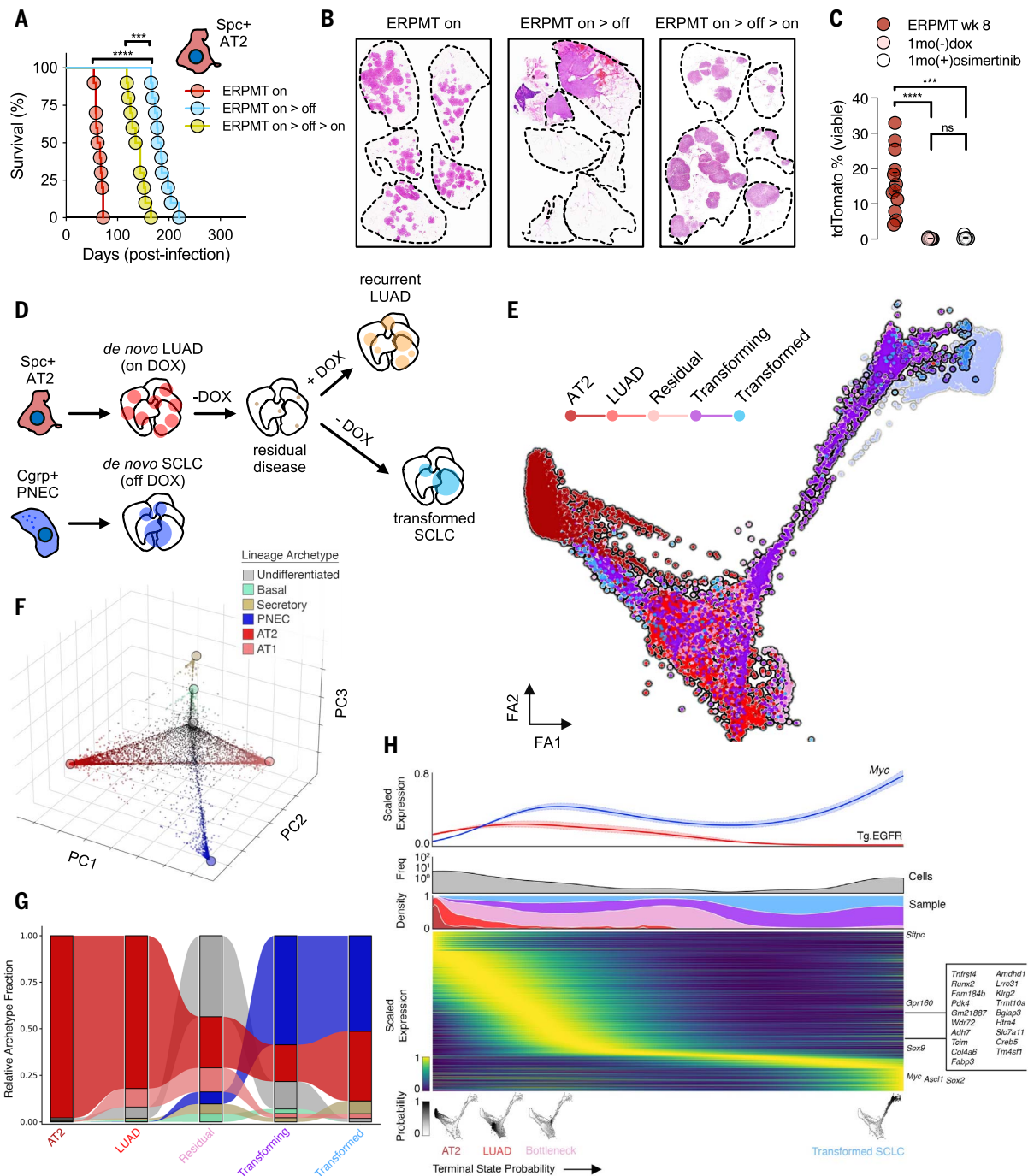


Fig. 2. Tracing the origins and transitions between LUAD and SCLC in vivo.

(A) Survival of AT2-derived ERPMT model on DOX (red), after DOX removal at 8 weeks (teal), and after restarting DOX diet 1 month after initial DOX removal (yellow; $n = 10$ mice per group); **** $P < 0.001$, **** $P < 0.0001$.

(B) Representative sagittal lung H&E sections from moribund mice in each group in (A). (C) tdTomato+ burden in the airway after 1 month of EGFR inhibition through DOX removal (pink; $n = 9$) or daily treatment with osimertinib (10 mg/kg; orally days 1 to 5 of 7; white; $n = 9$) as compared with 8 weeks time point before DOX removal (red; $n = 12$). DOX removal or osimertinib treatment (on DOX) were initiated at 8 weeks after the development of extensive ERPMT-derived LUAD tumorigenesis. For clarity, comparisons are effectively an 8-week pre-treatment cohort to ~12-week posttreatment cohorts (1 month of treatment); **** $P < 0.001$, **** $P < 0.0001$. (D) Outline of single-cell samples sequenced at

distinct time points along the transition between LUAD and SCLC after DOX perturbations [as described in (A)]. (E) Force-directed layout of cell states captured along the transition from an AT2 cell to ERPMT LUAD and lastly toward a neuroendocrine fate as compared with de novo SCLC tumorigenesis (transparent blue); colored by sample [annotated in (D); $n = 15,828$ cells pooled from three mice per sample]. FA, Force Atlas. (F) Principal components analysis (PCA) projection of the lung epithelial lineage probability space (see materials and methods) for all tumor-epithelial cells. Individual cells are colored by their max lineage probability, and archetypes are overlaid as colored nodes (fig. S4, C to E). (G) Flow plot showing relative abundance of cells assigned to their nearest lineage archetype, ordered by sampling time. (H) Heatmap of scaled imputed expression of highly variable transition genes (HVGs) (see materials and methods), top ranked macrostate genes, and lineage markers along terminal

cell-state probabilities computed with CellRank for all cells in (E). For each gene, expression was smoothed with a generalized additive model (GAM) as described in CellRank. The top HVGs correlated with the bottleneck macrostate (table S2) and select lineage-specific markers are labeled on the right. Above

the ranked heatmap are two KDEs showing relative sample abundance (lower) and total cell frequency (upper, gray). Above the KDEs are scaled imputed gene expression trends for the oncogenic drivers *Myc* and *EGFR*, modeled using a GAM along the terminal probability.

Cells expressing both *Ascl1* and *EGFR* were extremely rare, suggesting that a dual-positive state is either short-lived or unviable. Furthermore, independent of *Ascl1* expression, residual tumor cells retained expression of AT2 lineage markers and lacked high expression of a proliferative program characteristic of de novo SCLC (fig. S3C). These data provided the rationale to explore HT in our ERPMT model by extinguishing oncogenic EGFR transcriptionally through the withdrawal of DOX.

An undifferentiated, stem-like state emerges during HT

To generate conditions likely to favor HT, we removed DOX from ERPMT mice with late-stage LUAD and transcriptionally profiled single tdTom⁺ cells from pools of mice before, during, and after *EGFR* removal (Fig. 2D and materials and methods). We observed a continuous cell-state transition from a normal AT2 cell, through *EGFR*-driven LUAD, and finally toward transformed SCLC at later time points. A minority of tumor cells isolated from samples that were off DOX formed a bottleneck adjacent to the de novo LUAD model before breaking out toward transformed SCLC (Fig. 2E). Five extreme phenotypic states (“archetypes”; see materials and methods) (33) were identified that corresponded to mature lung epithelial lineages, including AT1, AT2, PNEC, secretory, and basal cell types; however, one archetype exhibited features of a highly undifferentiated state (Fig. 2F and fig. S4, A to C) and conspicuously mapped to the bottleneck between de novo LUAD and transformed SCLC (Fig. 2, F and G, and fig. S4, B to D). This undifferentiated archetype was not associated with any lung epithelial lineage but instead expressed relatively modest levels of basal-stem cell programs, as well as *Myc* and *Sox2* target genes (fig. S4C). It retained features of the original AT2 lineage and had not yet begun to express neuroendocrine markers, including *Ascl1* (fig. S4E). Tumor cells belonging to this undifferentiated state were a minority in primary LUAD, expanded in the residual LUAD (1 month off DOX), and diminished in the transforming (2 months off DOX) and transformed (>3 months off DOX) populations, which were composed largely of neuroendocrine tumor cells (Fig. 2G).

To model the transition from an AT2 cell of origin to an *EGFR*-driven LUAD, and lastly to a transformed neuroendocrine state, we applied CellRank (34) for single-cell fate mapping. Four stable cellular phenotypes (“macrostates”) were identified along this trajectory, capturing

normal AT2, de novo LUAD, the HT bottleneck, and then a transformed SCLC population, respectively (Fig. 2H, below heatmap). As the LUAD oncogenic driver was removed, MAPK pathway activity (35) expectedly decreased along this trajectory; conversely, we observed a time-dependent increase in *Myc* transcriptional output (table S2). Along this trajectory, a highly specific bottleneck to transformation emerged that was both stem-like (*Tmasf1*) (36, 37) and highly proliferative (38) and exhibited features of neuronal differentiation (*Creb*) (39–41) (Fig. 2H) and *Myc* downstream signaling (fig. S4F). Transcription factor regulatory modules (“regulons”) that characterize this bottleneck were likewise associated with neuronal plasticity (*Creb5*), airway stemness (*Sox9*), and basal-cell function (*Trp63*) (fig. S4G). Thus, on the path of HT, as levels of *EGFR* transcript wane, there may be selection for a cell state most fit to be driven by high levels of *Myc* (Fig. 2H and fig. S4F), and cells that break through this bottleneck may be rapidly transformed by *Myc* toward a neuroendocrine fate (Fig. 2H).

AT2 and PNEC lineage driver differences

To directly compare SCLC transformation efficiencies between AT2 and PNEC cells, we infected RPMT mice (which differ from ERPMT mice by lack of the oncogenic *EGFR* transgene) with equal titers of Ad5.Spc-Cre (for AT2) or Ad5.Cgrp-Cre (for PNEC). Initially, the tdTom⁺ frequency was greater in the airway of mice infected with Ad5.Spc-Cre, which is consistent with a higher baseline frequency of AT2 cells in the lung. However, this was short-lived and was followed by exponential expansion of the Ad5.Cgrp-Cre group (Fig. 3A). At 8 weeks after infection, macroscopic disease was clearly visible in the PNEC-derived RPMT model but not in the comparator (Fig. 3B).

To confirm whether our results with RPMT mice reflect the differential tolerance of cell lineages to the two oncogenic drivers, *Myc* and *EGFR*, we performed experiments in which production of a tamoxifen-activated Cre is governed by cell-specific promoters active in neuroendocrine (*Ascl1*^{CreERT2}) or AT2 (*Spc*^{CreERT2}) lineages, in the absence of Cre-susceptible loci for *Rbl* and *Trp53*. After tamoxifen administration to activate Cre^{ERT2}, we found that *Myc* expanded the airway *Ascl1*⁺ population and that *EGFR* led to an eventual decline. Conversely, *EGFR* expanded the AT2 lineage, whereas *Myc* was detrimental as compared with wild-type (WT) controls (Fig. 3C). In a larger cohort of mice, we observed that *Myc* expression alone from the *Ascl1*⁺ line-

age was sufficient to produce a lethal, fully penetrant phenotype, whereas *EGFR* was not. By contrast, *EGFR* expression alone was sufficient to transform the AT2 lineage, but *Myc* was not (Fig. 3D). These data strongly support cell lineage-specific differences in the tolerance of oncogenic drivers *Myc* and *EGFR* in the lung.

The pulmonary neuroendocrine cell is refractory to transformation by oncogenic EGFR

The phrase “terminal neuroendocrine” has been used to describe the eventual histology that the ERPMT model transitions toward following *EGFR* withdrawal; however, it was unclear whether this was a terminal state or if we could study HT in reverse by converting a SCLC tumor toward a LUAD state. As in earlier experiments, we initiated tumorigenesis from PNECs in the ERPMT model and followed cohorts of mice that were on or off DOX. There was a significant delay in the lethality of the model on DOX (fig. S5A); however, in the lungs of mice on DOX (where *EGFR* protein should be produced), we observed low-to-absent *EGFR* using immunohistochemistry (IHC) in tdTom⁺ tumor regions, which were histologically consistent with SCLC (fig. S5B). Immunofluorescence for *EGFR*^{L858R} and *Ascl1* showed patchy regions of *EGFR* positivity that were excluded from larger areas of *Ascl1* positivity (fig. S5C), with the *Ascl1*-positive/*EGFR*-negative SCLC component of these tumors being the most common in all mice examined. Taken together, these data support the conclusions that cells in the PNEC lineage resist transformation toward an *EGFR*-driven LUAD state, just as cells in the AT2 lineage cannot be easily transformed to SCLC, even though the latter form of HT can occasionally occur under select conditions.

Oncogenic *EGFR* led to a gradual elimination of PNECs over months, without evidence of acute intoxication (Fig. 3C). It was unclear whether elevated signaling through the MAPK pathway (through *EGFR*) was a disfavored situation for the PNEC or if *EGFR* incompatibility arose through some other mechanism. If excessive MAPK signaling suppressed PNEC proliferation, then inhibition of this pathway should increase *Ascl1*⁺ cells. To test this, we traced *Ascl1*⁺ cells and randomized mice to receive a diet formulated with or without the MAPK kinase inhibitor (MEKi) trametinib to suppress Mek>Erk signaling (fig. S6A). We terminated the study after 3 months on MEKi because of toxicity, with adult mice experiencing weight loss approaching our protocol limits (fig. S6B). However, no significant differences were

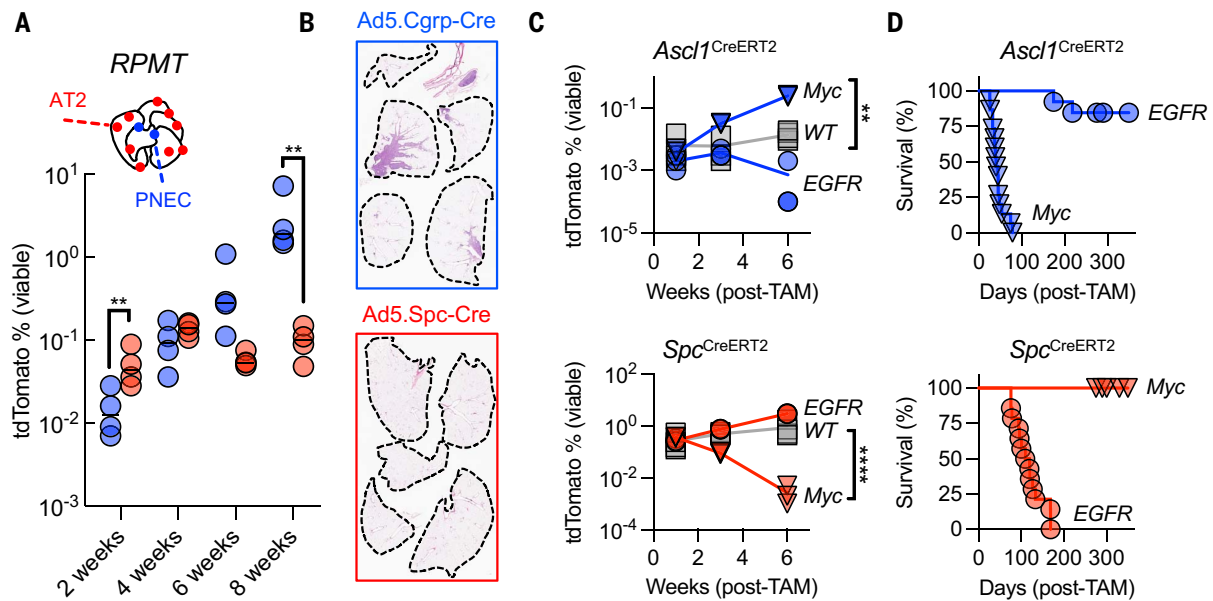


Fig. 3. Cell of origin and oncogenic driver incompatibility. (A) Frequency of tdTomato⁺ cells in the airway of RPMT mice after infection with equivalent titers of adenovirus ($\sim 10^6$ plaque-forming units per mouse) delivered using Ad5.Cgrp-Cre (blue) or Ad5.Spc-Cre (red) over a period of 8 weeks; $n = 4$ mice per time point; $**P < 0.01$. (B) Comparative histology of RPMT (no *Tg.TetO-EGFR^{L858R}* transgene) mice 8 weeks after infection with Ad5.Cgrp-Cre (blue outline) or Ad5.Spc-Cre (red outline). (C) Lineage-tracing oncogenic *Myc^{T58A}* (down-pointing triangles) or *EGFR^{L858R}*

(circles) on AT2 (*Spc^{CreERT2}*; red) or PNEC (*Ascl1^{CreERT2}*; blue) cells in the airway over time; $n = 3$ mice per time point. Control traces (tdTomato only; WT) are shown as gray squares; $**P < 0.01$, $****P < 0.0001$. (D) Long-term survival for cohorts shown in (C); (top) *Ascl1^{CreERT2} > EGFR^{L858R}* ($n = 13$) or *Myc^{T58A}* ($n = 15$) and (bottom) *Spc^{CreERT2} > EGFR^{L858R}* ($n = 14$) or *Myc^{T58A}* ($n = 12$). Mice having a single copy of *Rosa26^{LSL-tdTom}* and *Rosa26^{LSL-rtTA3}* were maintained on DOX chow throughout studies investigating lineage-trace allele-mediated expression of *Tg.TetO-EGFR^{L858R}*.

observed in the abundance of tdTom⁺ cells between the two cohorts (fig. S6C). Moreover, despite achieving chronic suppression of phospho-Erk signaling (fig. S6D), we did not observe any change in the location or proliferative status of tdTom⁺ cells in mice treated with the MEK1 diet (fig. S6E), suggesting that physiologic Mek>Erk signaling was not suppressing proliferation of PNECs.

Myc is sufficient to transform the PNEC

Lineage tracing demonstrated a clear difference in the sensitivity of the AT2 and PNEC cell types to oncogenic transformation by *Myc* (Fig. 3); however, a hallmark of SCLC is inactivation of the *RBI* and *TP53* tumor suppressors, in addition to heightened expression of a *Myc* family member and its transcriptional targets (7). Inspecting the bronchioles of mice expressing *Myc* driven by the *Ascl1^{CreERT2}* lineage trace (*Ascl1*>*Myc*) 1 month after labeling revealed clusters of proliferative tdTom⁺ cells that had not yet invaded surrounding tissues, which is consistent with carcinoma in situ (fig. S7A). Instead, all *Ascl1*>*Myc* mice were dying of cancer localized to the thyroid (fig. S7B). To date, we have been unsuccessful in activating the *Ascl1^{CreERT2}* allele specifically in the lungs, while sparing the trachea and thyroid. We therefore isolated tdTom⁺ cells from the airways of four distinct genotypes of mice combining *Ascl1* lineage-traced *Myc* with loss of *Rbi*, *Trp53*, or both tumor sup-

pressor genes. We expanded cells ex vivo using organotypic culture conditions and engrafted equivalent cell numbers into the flanks of athymic mice. Combined loss of *Rbi* and *Trp53* accelerated the growth of these *Myc*-driven tumors, but all genotypes were sufficient to form transplantable cancers. Moreover, all tumors had a similar histologic appearance consistent with high-grade neuroendocrine cancer (fig. S7C). These data suggest that PNECs could be transformed by *Myc* (alone) if expanded ex vivo, but this experiment did not demonstrate that *Myc* was required for tumor maintenance.

To test whether PNEC-derived tumors are dependent on *Myc*, we sorted tdTom⁺, rtTA3-expressing PNECs from the airway and infected cells with lentiviruses containing tetracycline promoter-driven *Myc* constructs. Coupling rtTA3 expression to the lineage trace (*Ascl1^{CreERT2}*) removed the likelihood of infecting lineage-negative cells present as contaminants. Although these cells were sparse (fig. S8), we could consistently generate organoid cultures from as few as 50 cells when DOX was present in the culture to drive the transcription of *Myc*. Removal of DOX resulted in near complete growth suppression of organoids expressing *Myc^{WT}* as compared with *Myc^{T58A}* (fig. S9, A to C), a long-lived version of *Myc* (42) (fig. S9C). Engrafting PNECs expressing inducible *Myc^{WT}* into athymic mice demonstrated DOX-dependent tumor growth. Removing DOX from tumor-

bearing mice dramatically reduced tumor volumes over the course of several weeks (fig. S9D), with residual fibrotic tumor tissue comprising noncycling cells (fig. S9E). Consistent with their rapid proliferation, *Myc*-driven PNEC organoids were sensitive to compounds that exacerbated replication stress, such as topoisomerase inhibitors (etoposide), as well as inhibitors of enzymes required for cell-cycle progression, including *Cdk4/6* (palbociclib) and *Wee1* (adavosertib) (fig. S9, F and G). Additionally, direct inhibition of the *Myc*-Max interface using the small molecule *Myci975* (43) provided similar reduction in organoid growth as compared with reduction resulting from DOX removal (fig. S9F).

AT2 cells are refractory to transformation by *Myc*

Although *Myc* alone may be sufficient to drive transformation and expansion of PNECs, our earlier results suggested that it was insufficient to transform the AT2 lineage (Fig. 3C). To further investigate what underlies this bottleneck, we established AT2 organoid cultures using recently published methods (44) from lineage-traced, WT, or *Myc^{T58A}*-expressing cells. These organoids expanded rapidly as compared with their WT counterparts but were unsustainable beyond three passages (fig. S10A). In early time points after the expression of *Myc^{T58A}* in AT2 cells in vivo, we noted incorporation of EdU in tdTom⁺ cells. However,

1 year after the initiation of the trace, tdTom⁺ cells in the airway failed to incorporate EdU, suggesting that they were no longer proliferative or were eliminated (fig. S10B). Ex vivo, AT2 organoids expressing *Myc*^{T58A} demonstrated increased DNA damage sensing, replication stress, and markers of programmed cell death as compared with WT (fig. S10C). It is unlikely that this resulted from an excess of Myc protein, because levels were lower in AT2 cells compared with levels tolerated in PNEC organoids (45) (fig. S10D). Lastly, consistent with the observation that Ras signaling through phosphatidylinositol-3-kinase (PI3K) relieves Myc-induced apoptosis (46), we likewise observed that Myc significantly accelerated oncogenic EGFR-driven LUAD, implying that enhanced signaling via the EGFR>Ras>Mek>Erk pathway can relieve intolerance to Myc in the AT2 lineage (fig. S10, E and F).

Although our data suggest that the different oncogenes driving AT2 and PNEC lineages are in stark contrast, it remained unclear whether other epithelial airway cells can transform in response to *Myc* alone. To address this, we performed a generalized, conditional trace using an *Nkx2.1*^{CreERT2} allele that will drive Cre-mediated recombination in a broad range of cell types derived from the anterior foregut endoderm, including the trachea, pituitary, thyroid, and most of the lung (47). At early time points, lineage-labeled tissues within the thyroid (both Ascl1⁺ and Ascl1⁻) expanded after *Myc* expression as compared with tissues in control mice (fig. S11A); however, at later time points there was outgrowth of tdTom⁺/Ascl1⁺ cells in bronchioles not observed in WT controls (fig. S11B). Together, these data suggest that the Ascl1⁺ PNEC is distinct in its tolerance to Myc, but we had not yet explained how intolerance to Myc could be overcome in the AT2 lineage during HT.

Deletion of *Pten* removes a barrier to *Myc* transformation

Genes up-regulated in tumor cells as they escaped the bottleneck to HT in our ERPMT model (termed “breakout”; fig. S12A) were notably associated with PI3K signaling (fig. S12, B and C) as compared with cells found in the bottleneck and not yet adopting neuroendocrine fate (48). Thus, we asked whether increasing PI3K-dependent Akt signaling through deletion of *Pten* would enable *Myc*^{T58A}-driven transformation in an AT2 lineage trace. Notably, we observed fully penetrant *Myc*-driven transformation in an AT2 cell (using *Spc*^{CreERT2}) when one copy of *Pten* was inactivated (*Spc*>*Pten*;Myc; Fig. 4A). At the median period when animals in the *Spc*>*Pten*;Myc cohort were moribund, lungs from *Spc*>Myc mice (*Pten*^{WT/WT}) showed no evidence of macroscopic disease (Fig. 4B). Similar observations were made when combining *Myc* expression with

a conditionally active, mutant *PI3K* allele (E545K) or inactivating both copies of *Pten* (*Pten*^{F1/F1}; Fig. 4B). Examining *Spc*>*Pten*;Myc animals 3 months after recombination reinforced the observation that lesions were variable in their frequency, size, and histologic appearance (fig. S13). However, they were Ascl1-negative and glandular in appearance, suggesting that they were adenocarcinoma-like and excluding the likelihood of SCLC, squamous, or mixed histology (fig. S13). AT2 lineage markers, including prosurfactant protein C (pro-SPC) and MHC Class II, were low or absent, and basal epithelial markers such as Sox2 and keratin 18 were variably expressed (fig. S13). Using scRNA-seq, we also observed a notable increase in the highly undifferentiated, basal stem-like state that followed combined loss of *Pten* and expression of *Myc* in AT2 cells—not seen with either genetic perturbation alone (Fig. 4C). Expectedly, this enrichment in the undifferentiated state was also associated with greater Myc transcriptional output (Fig. 4D).

Pulmonary basal cells efficiently generate SCLC

The basal stem-like program associated with AT2 cells capable of adaptation to *Myc* supported the possibility that an intermediate state during HT may be basal-like. More generally, this raised the possibility that the basal cell may serve as a cell of origin for SCLC, as speculated by others (49). However, targeting basal cells in mouse models is limited by their anatomic location, noted to be refractory to viral infections delivering Cre (50). Indeed, we observed an absence of tdTom⁺ cells in the lungs of mice 1 month after labeling when using a *Krt5*^{CreERT2} allele to target basal cells (fig. S14A). However, following regeneration in the proximal lung induced by naphthalene damage of secretory cells (51, 52), tdTom⁺ cells were detected within the lungs of mice, without a significant change in the trachea or thymus (fig. S14B). As basal cells are known to serve as multipotent progenitors (fig. S14C) (51–53), we then crossed mice to delete *Rb1* and/or *Trp53* from the basal lineage trace and found that *Rb1* loss alone was sufficient to skew cells toward a neuroendocrine fate (fig. S14D).

Consistent with this, we observed fully penetrant neuroendocrine tumorigenesis in mice that have lost both *Rb1* and *Trp53* with (*Krt5*>RPMT) or without (*Krt5*>RPT) expression of Myc from the basal lineage (fig. S14E); however, tumors arose with significantly shorter latency in mice expressing *Myc*. Expression of the conditional tdTomato reporter allele was easily observed throughout the keratinized epithelium of mice after recombination, but tumorigenesis was restricted to the proximal airway (fig. S14, F and H). Histologically, both models produced SCLC-like tumors; however, we noted that most tumors were adjacent to or within the thymus and did not invade the lungs unless we damaged

lungs with naphthalene (fig. S14, G to I). These data suggest that basal cells may serve not only as cells of origin for SCLC but also that basal-cell progeny and anatomic location can be influenced by genotype and injury.

An efficient model of AT2-derived SCLC after the loss of *Pten*

Deletion of *Pten* was sufficient to lower the barrier to transformation by Myc in the AT2 lineage; however, the resulting tumors were not neuroendocrine (fig. S13). We suspected that *Rb1* loss was required (10)—in addition to adaptation to Myc—for neuroendocrine transformation. Thus, to recapitulate bona fide transformation from an AT2 cell to SCLC efficiently, we generated a model in which we could delete *Rb1*, *Trp53*, and a copy of *Pten*, and express *Myc* and *tdTom* (*RPPTenMT*). If tumorigenesis was initiated in PNECs, there was no difference in latency between the RPMT and RPPTenMT models, but a significant difference emerged if the model was initiated in AT2 cells (Fig. 4E). AT2-derived RPPTenMT tumor cells displayed neuroendocrine expression profiles most similar to de novo SCLC (Fig. 4F and fig. S15, A and B). We also noted two subpopulations of cells stratified by expression of *Ascl1* (fig. S15B). Analysis of differential gene expression in the *Ascl1*^{low} group was notable for expression of neuronal genes, including *Stnm2*, *Nfix*, and *Maip1*. The *Ascl1*^{low} group also expressed high levels of *NeuroD1*, which is consistent with prior work showing *Myc* driving subtype plasticity from an Ascl1^{high} to Ascl1^{low}/NeuroD1^{high} transcriptional profile in multiple models of SCLC (54–58) (fig. S15C). Pathology revealed extensive heterogeneity with mixing of classic SCLC and large-cell neuroendocrine (LCNEC) tumor features, marked by variable expression of neuronal and neuroendocrine markers (fig. S15D).

Rb1 loss is necessary but insufficient for fully penetrant LUAD to SCLC transformation

The ERPMT model provided an efficient system to study HT, but we had not addressed a core requirement for Myc in this process. We generated another model in the absence of Myc overexpression (ERPT) and found that although some animals had recurrent disease after the removal of DOX (ERPT on > off), the penetrance of the phenotype was incomplete (Fig. 5A). Moreover, whereas the de novo ERPT LUAD showed an absence of Ascl1 and Myc protein, only some recurrent tumors appeared to be histologically consistent with SCLC, further limiting the utility of the ERPT model in recapitulating HT (Fig. 5, B to D). Although recurrence was incomplete, the ERPT tumors recurring as SCLC did show an increase in Myc protein (Fig. 5C). We analyzed the transcriptomes of ERPT and ERPMT LUAD tumor cells compared with those of normal AT2 cells and found that both the ERPT and ERPMT

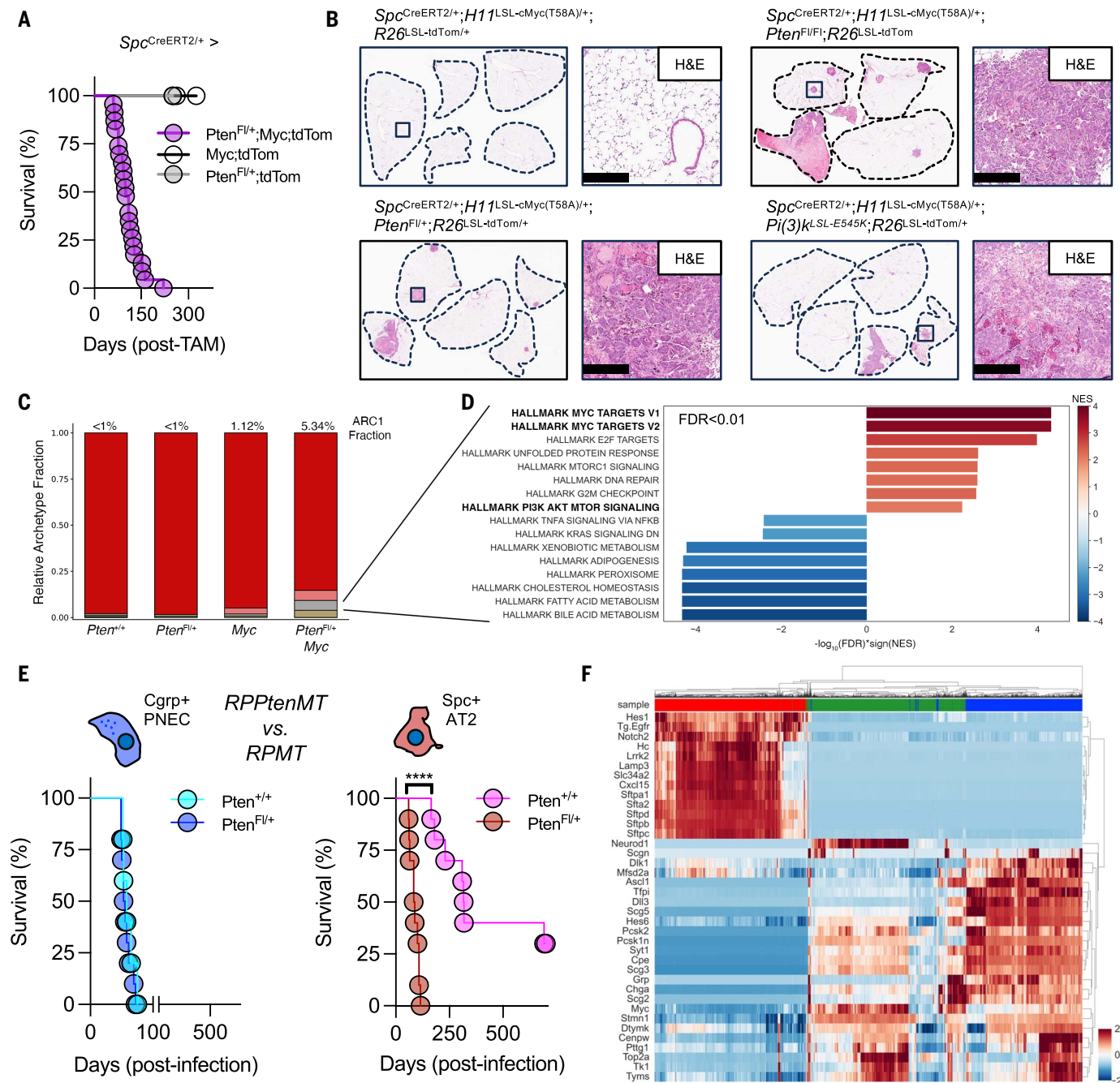


Fig. 4. Loss of *Pten* in the AT2 lineage removes the barrier to *Myc* transformation. (A) Survival of mice where *Myc* ($n = 12$), *Pten^{Fl/WT}* ($n = 5$), or the combination of these alleles ($n = 23$) are initiated in AT2 cells by using a single copy of *Spc^{CreERT2}*. Data were censored between 250 and 325 days in the nonlethal arms. (B) Comparative histology of whole lungs from representative *Spc>Myc*, *Spc>Pten^{Fl/+};Myc*, *Spc>Pten^{Fl/Fl};Myc*, or *Spc>P13K^L-E545K;Myc* mice at ~3 months after labeling. Higher-magnification regions (boxed) are provided at right; scalebars, 200 μ m. (C) Bar plot showing fraction of each epithelial lineage archetype detected per sample as in Fig. 2G. (D) Bar plot of hallmark gene sets

significantly enriched [false discovery rate (FDR) < 0.01] within the undifferentiated cell state of the *Spc>Pten^{Fl/+};Myc* sample pool. (E) Effect of *Pten* deletion combined with deletion of *p53* and *Rb1* and expression of *Myc* and *tdTomato* (RPPtenMT or RPMT) in neuroendocrine (blue) or AT2 (red) cells; $n = 10$ per arm with x axis split for clarity, **** $P < 0.0001$. (F) Clustered heatmap of z -normalized imputed expression of AT2 and PNEC signature genes and model oncogenic drivers (*Myc* and *Tg.EGFR*) for all tumor-epithelial cells from the RPPtenMT model (green) and the de novo LUAD (red) and SCLC (blue) models described in Fig. 1. Genes and cells are clustered by using the average Euclidean distance method.

models transcriptionally maintained expression of AT2 genes. However, *Myc* and embryonic stem cell target genes were elevated in the ERPT model and increased in the ERPMT

model, further supporting the role *Myc* over-expression has in HT after EGFR withdrawal (Fig. 5E). True paired cases of human LUAD before and after HT are limited, but some

studies have compared unrelated de novo LUAD with transformed SCLC (T-SCLC) in an attempt to understand this phenomenon as it relates to de novo SCLC tumorigenesis

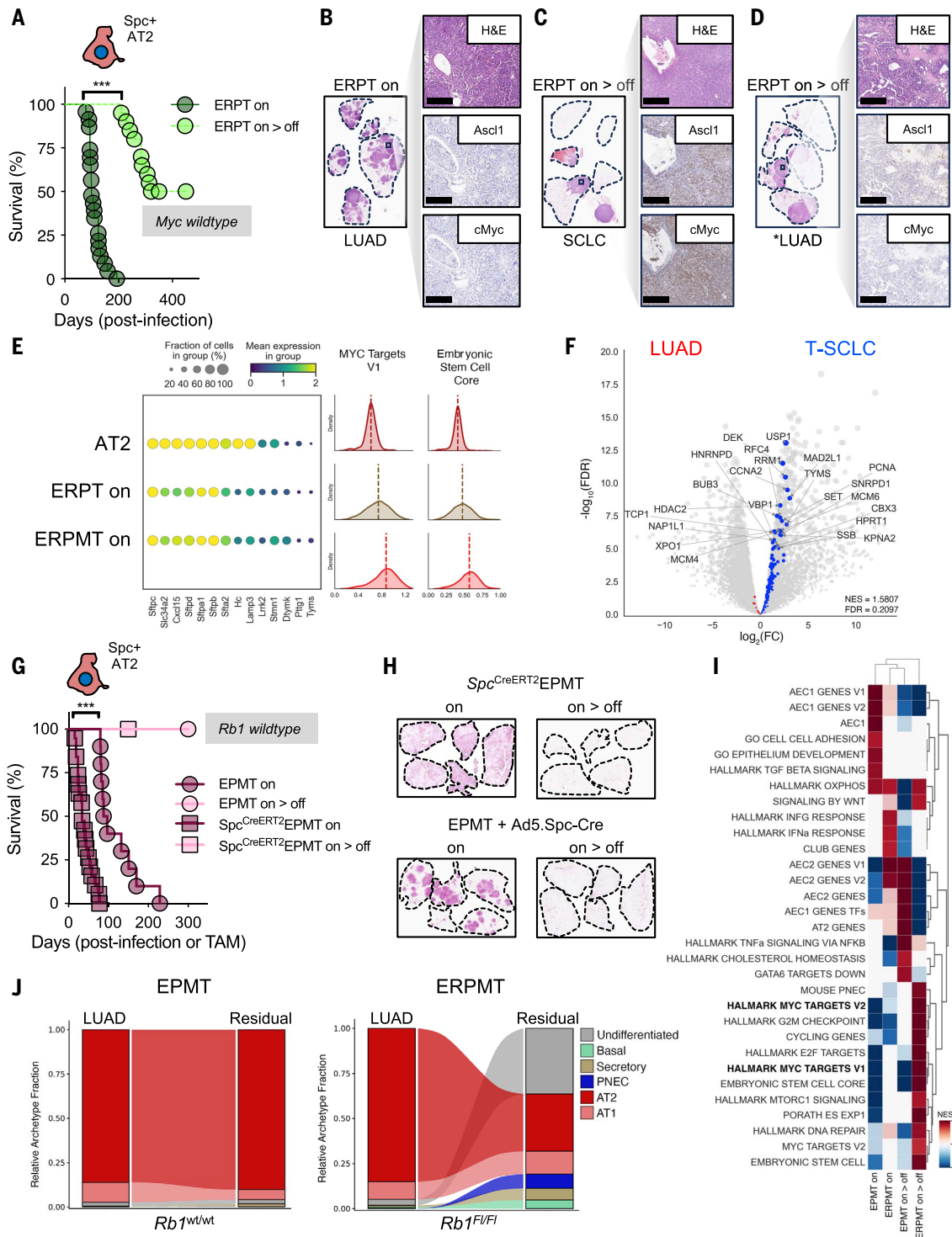


Fig. 5. Rb1 loss cooperates with Myc expression to facilitate HT.

(A) Survival of mice with the ERPT genotype (no *Myc*^{T58A} transgene) initiated with Ad5.Spc-Cre on DOX (ERPT on; dark green, *n* = 23), or on and then off DOX once mice developed advanced disease (ERPT on > off; light green, *n* = 20); ****P* < 0.001. As before, DOX diet was removed when individual mice exhibited signs of labored breathing and/or substantial weight loss with a hunched appearance. For each model, cohorts of mice were followed until approximately three times the median latency elapsed, at which point lungs were collected and the study was ended. (B) Histologic appearance of “ERPT on” lungs performed with H&E and IHC staining for Ascl1 and Myc (scalebar, 100 μm).

(C) Similar to (B), now with mice on and then off DOX, representative of a SCLC-like tumor. (D) As shown in (B), now with mice on and then off DOX, representative of a LUAD-like tumor. Pathologic interpretation is provided below each representative example. (E) (Left) Dot plot showing frequency of expressing cells (node size) and log-transformed expression (node color) of AT2 marker genes in normal AT2, ERPT LUAD, and ERPMT LUAD models. Genes shown are expressed in at least 25% of cells within at least one condition. (Right) KDE plots showing mean log-transformed expression by condition for select gene signatures. (F) Volcano plot showing differentially expressed genes from bulk RNAseq of human transformed SCLC versus LUAD. Genes from the

Hallmark *MYC* Targets V1 signature are colored according to conditional enrichment, top genes [abs(log₂FC) > 1 and FDR < 1 × 10⁻⁵, where “abs” is absolute and FC is “fold change”] are labeled, and the pathway normalized enrichment score (NES) and FDR from the gene set enrichment analysis (GSEA) are inset (bottom right). (G) Tumorigenesis initiated with an adenoviral (*n* = 10; Ad5.Spc-Cre) or AT2 lineage-trace allele (*n* = 19; *Spc*^{CreERT2}) in the EPMT model (*Rb1*^{WT/WT}) produces LUAD that does not relapse following DOX removal (*n* = 5 per group), ****P* < 0.001. (H) Representative sagittal lung H&E sections from each group in (G) on DOX at point of moribund disease or 1 month after the

removal of DOX from an otherwise moribund animal. (I) Clustered heatmap of gene signatures differentially enriched between the tumor-epithelial cells of the EPMT and ERPMT models before and after DOX removal. All pathways are significantly enriched (NES > 0 and FDR < 1 × 10⁻⁵) in at least one condition. Less significant signatures (FDR < 0.01) are transparent, and signatures not meeting this threshold are blank. Rows and columns are clustered by using the complete Manhattan distance method and metric. (J) Bar plot showing fraction of each epithelial lineage archetype detected per sample (as shown in Fig. 2G) for the EPMT (left) and ERPMT (right) models before and after removal of DOX.

(1, 3, 59, 60). We reanalyzed a publicly available cohort and could demonstrate that *Myc* target genes were differentially increased in T-SCLC as compared with LUAD, suggesting that *Myc* may have a role in facilitating HT in a clinical setting (Fig. 5F).

Rb1 loss cooperates with expression of *Myc* to facilitate neuroendocrine transformation

To compare the relative dependence of *Rb1* loss and *Myc* overexpression for HT, we generated a model in which *Rb1* was WT (EPMT) and initiated tumorigenesis in AT2 cells using Ad5.Spc-Cre or a lineage trace (*Spc*^{CreERT2}-EPMT). If on DOX, then both models produced LUAD with differences in latency likely reflecting the broad initiation achievable when using a lineage-trace allele as compared with sparse infection using inhaled adenovirus. (Fig. 5, G and H). LUAD did not recur in EPMT mice taken off DOX. Through a comparison of de novo LUAD and off-DOX residual cells from tumors of varying *Rb1* status, we observed marked up-regulation of transcriptional programs associated with HT after DOX removal that were dependent on loss of *Rb1* (Fig. 5I). Additionally, the relative abundance of lineage archetypes shifts within these models in response to DOX removal suggests that, in the presence of *Rb1* loss, high *Myc* expression selects for a residual state that is stem-like and capable of full neuroendocrine transformation (Fig. 5J). Thus, these events cooperate, as neither *Rb1* loss nor *Myc* overexpression alone are sufficient for fully penetrant HT.

We conclude that the AT2 cell is highly refractory to transformation by oncogenic *Myc*, as are many other cell types within the lung, the noted exception being the PNEC. Intolerance of AT2 cells to *Myc* can be relieved through activation of the Akt signaling pathway, such as through the deletion of the tumor suppressor *Pten*. Although this generates a permissive stem-like state, the full conversion to a *Myc*-driven, high-grade neuroendocrine cancer requires the additional loss of *Rb1*.

Discussion

Carcinogenesis and related processes, such as tumor progression, therapy resistance, and HT, remain incompletely understood. To understand the mechanism by which HT occurs in lung cancer, we have developed mouse models in

which lung tumorigenesis can be initiated in different cell lineages to follow the transformation of EGFR-driven LUAD to *Myc*-driven SCLC. In doing so, we demonstrate that HT can be simplified conceptually to a change in oncogenic drivers as the tumor cells transition between states that resemble cells in the AT2 and the PNEC lineages. The driver oncogene in the PNEC lineage is *Myc*, and the bottleneck in HT can be relieved by mechanisms that allow an AT2 cell to become stem-like and capable of tolerating *Myc* as an oncogenic driver.

Understanding the events that facilitate HT clinically has been limited by the lack of samples obtained from the same patient before, during, and after HT. Comparisons of de novo SCLC to transformed SCLC have highlighted pathways activated after neuroendocrine differentiation (59). A more recent study relied on putative HT samples in which a LUAD oncogenic driver was detected in a histologically confirmed SCLC. When compared to de novo SCLC, these cases were enriched for mutations that activate the PI3K signaling pathway (61). Consistent with this result, we found that loss of *Pten* or activation of *Pik3ca* was sufficient to break a barrier in the AT2 lineage to transformation by *Myc* but insufficient to lead to neuroendocrine transformation.

Previous work has established a combination of genetic events capable of reprogramming human cell types to neuroendocrine cancers (62); however, the intermediate steps in this process remain unclear. We have built upon this foundational work by developing intact genetically engineered animals and sampling tumor cells throughout the lifetime of HT. Moreover, our findings show that although *Rb1* loss is necessary for HT to a neuroendocrine cancer, it is the extinction of the driver oncogene transcriptionally that is required before the emergence of neuroendocrine features.

Beyond the genetic manipulations and changes in gene expression described here, we speculate that there are likely other mechanisms that allow for such lineage conversion, cellular plasticity, or transdifferentiation. Lineage tracing has demonstrated that basal progenitors can give rise to PNECs (63, 64). More recently, tracheal basal cells have been shown to differentiate toward a PNEC fate under hypoxic conditions, but the intermediate transcriptional steps in this complex process are uncharted (65).

In our attempts to describe the transition state between LUAD and SCLC, we found that these tumor cells appear “basal-like” on the basis of their transcriptional profile but lack definitive basal lineage markers. Instead, these cells are more accurately described as “lineage negative,” stem-like progenitors. Such cells have been described to arise in the mouse lung following major airway injury (66). Thus, the airway cell most capable of such plasticity may be the pulmonary basal cell or a stem-like cell that has yet to be fully characterized.

Lastly, it is unclear whether therapeutic targeting of pathways facilitating HT in patients poised to undergo HT will be efficacious. Our results suggest that noninvasive monitoring for activation of the Akt signaling pathway (such as the appearance of *PI3K* mutations in circulating tumor DNA) may serve to alert physicians to the likelihood of HT before the emergence of an aggressive, transformed SCLC. It is not yet known whether direct targeting of *Myc* in such *Myc*-driven scenarios (including HT or de novo SCLC tumorigenesis) will be fruitful; however, strategies to inhibit the transcriptional activity of *Myc* proteins have advanced substantially over the last decade and might ultimately have clinical utility in multiple contexts (43, 67, 68).

Limitations of the study

There are several key limitations to this study. First, we are attempting to understand HT by modeling a human phenomenon in the mouse, where the complexity of cell types and microenvironments is not identical to that found in humans. Recent descriptions of the human distal airway have found a diversity of cell types in human lungs that are not observed in the mouse, including specialized regenerative cells with hybrid alveolar-secretory character and multiple subtypes of basal cells (19, 69, 70). For example, basal cells are not present in the mouse lung unless the airway is damaged, which we demonstrated using naphthalene. Furthermore, most laboratory mice are housed under pathogen-free conditions. We know that lifetime exposure to various carcinogens and particulates fundamentally alters the microenvironment of the lung, including the likelihood that a cancer may develop (71, 72). Second, there are processes in human cells not found in the mouse that may be critical for HT, including the role for

APOBEC-mediated hypermutation. Studies of EGFR-mutated LUAD have found APOBEC mutagenesis signatures after treatment with EGFR-targeted therapies (11, 73, 74), and this mutational signature is enriched after HT (1, 61). It is unclear whether APOBEC mutations are directly responsible for activating the PI3K signaling pathway, (hypothetically) relieving intolerance of the AT2 cell to Myc (1, 59, 61); however, other studies would suggest that this is possible (75, 76). Lastly, we were unable to initiate tumorigenesis in the ERPMT model with the *SpC*^{CreERT2} allele. This proved impossible because in the mouse genome, the *Rbl* locus is ~3 Mb from the *Sftpc* locus (GRCm38/mm10). Such proximity precludes generation of the desired genotype with both homozygous floxed copies of *Rbl* and the *SpC*^{CreERT2} lineage-trace allele.

REFERENCES AND NOTES

- J. K. Lee et al., Clonal History and Genetic Predictors of Transformation Into Small-Cell Carcinomas From Lung Adenocarcinomas. *J. Clin. Oncol.* **35**, 3065–3074 (2017). doi: [10.1200/JCO.2016.71.9096](https://doi.org/10.1200/JCO.2016.71.9096); pmid: [28498782](https://pubmed.ncbi.nlm.nih.gov/28498782/)
- M. F. Zakowski, M. Ladanyi, M. G. Kris; Memorial Sloan-Kettering Cancer Center Lung Cancer OncoGenome Group, EGFR mutations in small-cell lung cancers in patients who have never smoked. *N. Engl. J. Med.* **355**, 213–215 (2006). doi: [10.1056/NEJM053610](https://doi.org/10.1056/NEJM053610); pmid: [16837691](https://pubmed.ncbi.nlm.nih.gov/16837691/)
- L. V. Sequist et al., Genotypic and histological evolution of lung cancers acquiring resistance to EGFR inhibitors. *Sci. Transl. Med.* **3**, 75ra26 (2011). doi: [10.1126/scitranslmed.3002003](https://doi.org/10.1126/scitranslmed.3002003); pmid: [21430269](https://pubmed.ncbi.nlm.nih.gov/21430269/)
- H. Beltran et al., Divergent clonal evolution of castration-resistant neuroendocrine prostate cancer. *Nat. Med.* **22**, 298–305 (2016). doi: [10.1038/nm.4045](https://doi.org/10.1038/nm.4045); pmid: [26855148](https://pubmed.ncbi.nlm.nih.gov/26855148/)
- D. Hirano, Y. Okada, S. Minei, Y. Takimoto, N. Nemoto, Neuroendocrine differentiation in hormone refractory prostate cancer following androgen deprivation therapy. *Eur. Urol.* **45**, 586–592, discussion 592 (2004). doi: [10.1016/j.eururo.2003.11.032](https://doi.org/10.1016/j.eururo.2003.11.032); pmid: [15082200](https://pubmed.ncbi.nlm.nih.gov/15082200/)
- Á. Quintana-Villalonga et al., Lineage plasticity in cancer: A shared pathway of therapeutic resistance. *Nat. Rev. Clin. Oncol.* **17**, 360–371 (2020). doi: [10.1038/s41571-020-0340-z](https://doi.org/10.1038/s41571-020-0340-z); pmid: [32152485](https://pubmed.ncbi.nlm.nih.gov/32152485/)
- J. George et al., Comprehensive genomic profiles of small cell lung cancer. *Nature* **524**, 47–53 (2015). doi: [10.1038/nature14664](https://doi.org/10.1038/nature14664); pmid: [26168399](https://pubmed.ncbi.nlm.nih.gov/26168399/)
- C. M. Rudin et al., Molecular subtypes of small cell lung cancer: A synthesis of human and mouse model data. *Nat. Rev. Cancer* **19**, 289–297 (2019). doi: [10.1038/s41568-019-0133-9](https://doi.org/10.1038/s41568-019-0133-9); pmid: [30926931](https://pubmed.ncbi.nlm.nih.gov/30926931/)
- M. G. Oser, M. J. Niederst, L. V. Sequist, J. A. Engelman, Transformation from non-small-cell lung cancer to small-cell lung cancer: Molecular drivers and cells of origin. *Lancet Oncol.* **16**, e165–e172 (2015). doi: [10.1016/S1470-2045\(14\)71180-5](https://doi.org/10.1016/S1470-2045(14)71180-5); pmid: [25846096](https://pubmed.ncbi.nlm.nih.gov/25846096/)
- M. J. Niederst et al., RB loss in resistant EGFR mutant lung adenocarcinomas that transform to small-cell lung cancer. *Nat. Commun.* **6**, 6377 (2015). doi: [10.1038/ncomms7377](https://doi.org/10.1038/ncomms7377); pmid: [25758528](https://pubmed.ncbi.nlm.nih.gov/25758528/)
- M. Offin et al., Concurrent RB1 and TP53 Alterations Define a Subset of EGFR-Mutant Lung Cancers at Risk for Histologic Transformation and Inferior Clinical Outcomes. *J. Thorac. Oncol.* **14**, 1784–1793 (2019). doi: [10.1016/j.jtho.2019.06.002](https://doi.org/10.1016/j.jtho.2019.06.002); pmid: [31228622](https://pubmed.ncbi.nlm.nih.gov/31228622/)
- T. J. Desai, D. G. Brownfield, M. A. Krasnow, Alveolar progenitor and stem cells in lung development, renewal and cancer. *Nature* **507**, 190–194 (2014). doi: [10.1038/nature12930](https://doi.org/10.1038/nature12930); pmid: [24499815](https://pubmed.ncbi.nlm.nih.gov/24499815/)
- D. B. Frank et al., Early lineage specification defines alveolar epithelial ontogeny in the murine lung. *Proc. Natl. Acad. Sci. U.S.A.* **116**, 4362–4371 (2019). doi: [10.1073/pnas.1813952116](https://doi.org/10.1073/pnas.1813952116); pmid: [30782824](https://pubmed.ncbi.nlm.nih.gov/30782824/)
- A. N. Nabhan, D. G. Brownfield, P. B. Harbury, M. A. Krasnow, T. J. Desai, Single-cell Wnt signaling niches maintain stemness of alveolar type 2 cells. *Science* **359**, 1118–1123 (2018). doi: [10.1126/science.aam6603](https://doi.org/10.1126/science.aam6603); pmid: [29420258](https://pubmed.ncbi.nlm.nih.gov/29420258/)
- Cancer Genome Atlas Research Network, Comprehensive molecular profiling of lung adenocarcinoma. *Nature* **511**, 543–550 (2014). doi: [10.1038/nature13385](https://doi.org/10.1038/nature13385); pmid: [25079552](https://pubmed.ncbi.nlm.nih.gov/25079552/)
- Y. Ouadah et al., Rare Pulmonary Neuroendocrine Cells Are Stem Cells Regulated by Rb, p53, and Notch. *Cell* **179**, 403–416.e23 (2019). doi: [10.1016/j.cell.2019.09.010](https://doi.org/10.1016/j.cell.2019.09.010); pmid: [31585080](https://pubmed.ncbi.nlm.nih.gov/31585080/)
- C. S. Kuo, M. A. Krasnow, Formation of a Neurosensory Organ by Epithelial Cell Slithering. *Cell* **163**, 394–405 (2015). doi: [10.1016/j.cell.2015.09.021](https://doi.org/10.1016/j.cell.2015.09.021); pmid: [26435104](https://pubmed.ncbi.nlm.nih.gov/26435104/)
- P. Sui et al., Pulmonary neuroendocrine cells amplify allergic asthma responses. *Science* **360**, ean8546 (2018). doi: [10.1126/science.aan8546](https://doi.org/10.1126/science.aan8546); pmid: [29599193](https://pubmed.ncbi.nlm.nih.gov/29599193/)
- K. J. Travaglini et al., A molecular cell atlas of the human lung from single-cell RNA sequencing. *Nature* **587**, 619–625 (2020). doi: [10.1038/s41586-020-2922-4](https://doi.org/10.1038/s41586-020-2922-4); pmid: [33208946](https://pubmed.ncbi.nlm.nih.gov/33208946/)
- K. Politi et al., Lung adenocarcinomas induced in mice by mutant EGF receptors found in human lung cancers respond to a tyrosine kinase inhibitor or to down-regulation of the receptors. *Genes Dev.* **20**, 1496–1510 (2006). doi: [10.1101/gad.1417406](https://doi.org/10.1101/gad.1417406); pmid: [16705038](https://pubmed.ncbi.nlm.nih.gov/16705038/)
- K. D. Sutherland et al., Cell of origin of small cell lung cancer: Inactivation of Trp53 and Rbl in distinct cell types of adult mouse lung. *Cancer Cell* **19**, 754–764 (2011). doi: [10.1016/j.ccr.2011.04.019](https://doi.org/10.1016/j.ccr.2011.04.019); pmid: [21665149](https://pubmed.ncbi.nlm.nih.gov/21665149/)
- C. E. Barkauskas et al., Type 2 alveolar cells are stem cells in adult lung. *J. Clin. Invest.* **123**, 3025–3036 (2013). doi: [10.1172/JCI68782](https://doi.org/10.1172/JCI68782); pmid: [23921127](https://pubmed.ncbi.nlm.nih.gov/23921127/)
- A. M. Laughney et al., Regenerative lineages and immune-mediated pruning in lung cancer metastasis. *Nat. Med.* **26**, 259–269 (2020). doi: [10.1038/s41591-019-0750-6](https://doi.org/10.1038/s41591-019-0750-6); pmid: [32042191](https://pubmed.ncbi.nlm.nih.gov/32042191/)
- Y. He et al., MHC class II expression in lung cancer. *Lung Cancer* **112**, 75–80 (2017). doi: [10.1016/j.lungcan.2017.07.030](https://doi.org/10.1016/j.lungcan.2017.07.030); pmid: [29191604](https://pubmed.ncbi.nlm.nih.gov/29191604/)
- T. Yazawa et al., Lack of class II transactivator causes severe deficiency of HLA-DR expression in small cell lung cancer. *J. Pathol.* **187**, 191–199 (1999). doi: [10.1002/\(SICI\)1096-9896\(199901\)187:2<191::AID-PATH206>3.0.CO;2-3](https://doi.org/10.1002/(SICI)1096-9896(199901)187:2<191::AID-PATH206>3.0.CO;2-3); pmid: [10365094](https://pubmed.ncbi.nlm.nih.gov/10365094/)
- L. M. Marsh et al., Surface expression of CD74 by type II alveolar epithelial cells: A potential mechanism for macrophage migration inhibitory factor-induced epithelial repair. *Am. J. Physiol. Lung Cell. Mol. Physiol.* **296**, L442–L452 (2009). doi: [10.1152/ajplung.00525.2007](https://doi.org/10.1152/ajplung.00525.2007); pmid: [19136583](https://pubmed.ncbi.nlm.nih.gov/19136583/)
- S. Bae, Y. Bessho, M. Hojo, R. Kageyama, The bHLH gene Hes6, an inhibitor of Hes1, promotes neuronal differentiation. *Development* **127**, 2933–2943 (2000). doi: [10.1242/dev.127.13.2933](https://doi.org/10.1242/dev.127.13.2933); pmid: [10851137](https://pubmed.ncbi.nlm.nih.gov/10851137/)
- J. D. Buenrostro, B. Wu, H. Y. Chang, W. J. Greenleaf, ATAC-seq: A Method for Assaying Chromatin Accessibility Genome-Wide. *Curr. Protoc. Mol. Biol.* **109**, 21.29–21.9.9 (2015). doi: [10.1002/0471142727.mb2129s109](https://doi.org/10.1002/0471142727.mb2129s109); pmid: [25559105](https://pubmed.ncbi.nlm.nih.gov/25559105/)
- P. A. Ewels et al., The nf-core framework for community-curated bioinformatics pipelines. *Nat. Biotechnol.* **38**, 276–278 (2020). doi: [10.1038/s41587-020-0439-x](https://doi.org/10.1038/s41587-020-0439-x); pmid: [32055031](https://pubmed.ncbi.nlm.nih.gov/32055031/)
- S. Heinz et al., Simple combinations of lineage-determining transcription factors prime cis-regulatory elements required for macrophage and B cell identities. *Mol. Cell* **38**, 576–589 (2010). doi: [10.1016/j.molcel.2010.05.004](https://doi.org/10.1016/j.molcel.2010.05.004); pmid: [20513432](https://pubmed.ncbi.nlm.nih.gov/20513432/)
- Y. Oren et al., Cycling cancer persister cells arise from lineages with distinct programs. *Nature* **596**, 576–582 (2021). doi: [10.1038/s41586-021-03796-6](https://doi.org/10.1038/s41586-021-03796-6); pmid: [34381210](https://pubmed.ncbi.nlm.nih.gov/34381210/)
- M. D. Borromeo et al., ASCL1 and NEUROD1 Reveal Heterogeneity in Pulmonary Neuroendocrine Tumors and Regulate Distinct Genetic Programs. *Cell Rep.* **16**, 1259–1272 (2016). doi: [10.1016/j.celrep.2016.06.081](https://doi.org/10.1016/j.celrep.2016.06.081); pmid: [27452466](https://pubmed.ncbi.nlm.nih.gov/27452466/)
- A. Cutler, L. Breiman, Archetypal Analysis. *Technometrics* **36**, 338–347 (1994). doi: [10.1080/00401706.1994.10485840](https://doi.org/10.1080/00401706.1994.10485840)
- M. Lange et al., CellRank for directed single-cell fate mapping. *Nat. Methods* **19**, 159–170 (2022). doi: [10.1038/s41592-021-01346-6](https://doi.org/10.1038/s41592-021-01346-6); pmid: [35027767](https://pubmed.ncbi.nlm.nih.gov/35027767/)
- M. C. Wagle et al., A transcriptional MAPK Pathway Activity Score (MPAS) is a clinically relevant biomarker in multiple cancer types. *NPJ Precis. Oncol.* **2**, 7 (2018). doi: [10.1038/s41698-018-0051-4](https://doi.org/10.1038/s41698-018-0051-4); pmid: [29872725](https://pubmed.ncbi.nlm.nih.gov/29872725/)
- G. Chen et al., Targeting TM4SF1 exhibits therapeutic potential via inhibition of cancer stem cells. *Signal Transduct. Target. Ther.* **7**, 350 (2022). doi: [10.1038/s41392-022-01177-7](https://doi.org/10.1038/s41392-022-01177-7); pmid: [36229443](https://pubmed.ncbi.nlm.nih.gov/36229443/)
- X. Ouyang et al., WDR72 Enhances the Stemness of Lung Cancer Cells by Activating the AKT/HIF-1 α Signaling Pathway. *J. Oncol.* **2022**, 5059588 (2022). doi: [10.1155/2022/5059588](https://doi.org/10.1155/2022/5059588); pmid: [36385964](https://pubmed.ncbi.nlm.nih.gov/36385964/)
- M. S. Kowalczyk et al., Single-cell RNA-seq reveals changes in cell cycle and differentiation programs upon aging of hematopoietic stem cells. *Genome Res.* **25**, 1860–1872 (2015). doi: [10.1101/gr.192237.115](https://doi.org/10.1101/gr.192237.115); pmid: [26430063](https://pubmed.ncbi.nlm.nih.gov/26430063/)
- N. Tsuboyama et al., Therapeutic targeting of BAP1/ASXL3 sub-complex in ASCL1-dependent small cell lung cancer. *Oncogene* **41**, 2152–2162 (2022). doi: [10.1038/s41388-022-02240-x](https://doi.org/10.1038/s41388-022-02240-x); pmid: [35194152](https://pubmed.ncbi.nlm.nih.gov/35194152/)
- Z. Zhao et al., PAI9 Determines Epigenetic State Transition and Cell Fate in Cancer. *Cancer Res.* **81**, 4696–4708 (2021). doi: [10.1158/0008-5472.CAN-21-1114](https://doi.org/10.1158/0008-5472.CAN-21-1114); pmid: [34341073](https://pubmed.ncbi.nlm.nih.gov/34341073/)
- Y. Xia et al., Targeting CREB Pathway Suppresses Small Cell Lung Cancer. *Mol. Cancer Res.* **16**, 825–832 (2018). doi: [10.1158/1541-7786.MCR-17-0576](https://doi.org/10.1158/1541-7786.MCR-17-0576); pmid: [29523765](https://pubmed.ncbi.nlm.nih.gov/29523765/)
- M. A. Gregory, Y. Qi, S. R. Hann, Phosphorylation by glycogen synthase kinase-3 controls c-myc proteolysis and subnuclear localization. *J. Biol. Chem.* **278**, 51606–51612 (2003). doi: [10.1074/jbc.M310722200](https://doi.org/10.1074/jbc.M310722200); pmid: [14563837](https://pubmed.ncbi.nlm.nih.gov/14563837/)
- H. Han et al., Small-Molecule MYC Inhibitors Suppress Tumor Growth and Enhance Immunotherapy. *Cancer Cell* **36**, 483–497.e15 (2019). doi: [10.1016/j.ccell.2019.10.001](https://doi.org/10.1016/j.ccell.2019.10.001); pmid: [31679823](https://pubmed.ncbi.nlm.nih.gov/31679823/)
- S. Naranzo et al., Modeling diverse genetic subtypes of lung adenocarcinoma with a next-generation alveolar type 2 organoid platform. *Genes Dev.* **36**, 936–949 (2022). doi: [10.1101/gad.349659.122](https://doi.org/10.1101/gad.349659.122); pmid: [36175034](https://pubmed.ncbi.nlm.nih.gov/36175034/)
- D. J. Murphy et al., Distinct thresholds govern Myc's biological output in vivo. *Cancer Cell* **14**, 447–457 (2008). doi: [10.1016/j.ccr.2008.10.018](https://doi.org/10.1016/j.ccr.2008.10.018); pmid: [19061836](https://pubmed.ncbi.nlm.nih.gov/19061836/)
- A. Kauffmann-Zeh et al., Suppression of c-Myc-induced apoptosis by Ras signalling through PI(3)K and PKB. *Nature* **385**, 544–548 (1997). doi: [10.1038/385544a0](https://doi.org/10.1038/385544a0); pmid: [9020362](https://pubmed.ncbi.nlm.nih.gov/9020362/)
- H. Taniguchi et al., A resource of Cre driver lines for genetic targeting of GABAergic neurons in cerebral cortex. *Neuron* **71**, 995–1013 (2011). doi: [10.1016/j.neuron.2011.07.026](https://doi.org/10.1016/j.neuron.2011.07.026); pmid: [21943598](https://pubmed.ncbi.nlm.nih.gov/21943598/)
- E. Y. Chen et al., Enrichr: Interactive and collaborative HTML5 gene list enrichment analysis tool. *BMC Bioinformatics* **14**, 128 (2013). doi: [10.1186/1471-2105-14-128](https://doi.org/10.1186/1471-2105-14-128); pmid: [23586463](https://pubmed.ncbi.nlm.nih.gov/23586463/)
- S. Lázaro et al., Differential development of large-cell neuroendocrine or small-cell lung carcinoma upon inactivation of 4 tumor suppressor genes. *Proc. Natl. Acad. Sci. U.S.A.* **116**, 22300–22306 (2019). doi: [10.1073/pnas.1821745116](https://doi.org/10.1073/pnas.1821745116); pmid: [31611390](https://pubmed.ncbi.nlm.nih.gov/31611390/)
- G. Ferone et al., SOX2 Is the Determining Oncogenic Switch in Promoting Lung Squamous Cell Carcinoma from Different Cells of Origin. *Cancer Cell* **30**, 519–532 (2016). doi: [10.1016/j.ccell.2016.09.001](https://doi.org/10.1016/j.ccell.2016.09.001); pmid: [27728803](https://pubmed.ncbi.nlm.nih.gov/27728803/)
- J. R. Rock et al., Basal cells as stem cells of the mouse trachea and human airway epithelium. *Proc. Natl. Acad. Sci. U.S.A.* **106**, 12771–12775 (2009). doi: [10.1073/pnas.0906850106](https://doi.org/10.1073/pnas.0906850106); pmid: [19625615](https://pubmed.ncbi.nlm.nih.gov/19625615/)
- K. U. Hong, S. D. Reynolds, S. Watkins, E. Fuchs, B. R. Stripp, Basal cells are a multipotent progenitor capable of renewing the bronchial epithelium. *Am. J. Pathol.* **164**, 577–588 (2004). doi: [10.1016/S0002-9440\(10\)63147-1](https://doi.org/10.1016/S0002-9440(10)63147-1); pmid: [14742263](https://pubmed.ncbi.nlm.nih.gov/14742263/)
- B. Hogan, P. R. Tata, Cellular organization and biology of the respiratory system. *Nat. Cell Biol.* (2019). doi: [10.1038/s41556-019-0357-7](https://doi.org/10.1038/s41556-019-0357-7); pmid: [31346286](https://pubmed.ncbi.nlm.nih.gov/31346286/)
- A. S. Ireland et al., MYC Drives Temporal Evolution of Small Cell Lung Cancer Subtypes by Reprogramming Neuroendocrine Fate. *Cancer Cell* **38**, 60–78.e12 (2020). doi: [10.1016/j.ccell.2020.05.001](https://doi.org/10.1016/j.ccell.2020.05.001); pmid: [32473656](https://pubmed.ncbi.nlm.nih.gov/32473656/)
- R. R. Olsen et al., ASCL1 represses a SOX9⁺ neural crest stem-like state in small cell lung cancer. *Genes Dev.* **35**, 847–869 (2021). doi: [10.1101/gad.348295.121](https://doi.org/10.1101/gad.348295.121); pmid: [34016693](https://pubmed.ncbi.nlm.nih.gov/34016693/)
- D. Lissa et al., Heterogeneity of neuroendocrine transcriptional states in metastatic small cell lung cancers and patient-derived models. *Nat. Commun.* **13**, 2023 (2022). doi: [10.1038/s41467-022-29517-9](https://doi.org/10.1038/s41467-022-29517-9); pmid: [35440132](https://pubmed.ncbi.nlm.nih.gov/35440132/)
- J. M. Chan et al., Signatures of plasticity, metastasis, and immunosuppression in an atlas of human small cell lung cancer. *Cancer Cell* **39**, 1479–1496.e18 (2021). doi: [10.1016/j.ccell.2021.09.008](https://doi.org/10.1016/j.ccell.2021.09.008); pmid: [34653364](https://pubmed.ncbi.nlm.nih.gov/34653364/)
- C. M. Gay et al., Patterns of transcription factor programs and immune pathway activation define four major subtypes of SCLC with distinct therapeutic vulnerabilities. *Cancer Cell* **39**,

- 346–360.e7 (2021). doi: [10.1016/j.ccell.2020.12.014](https://doi.org/10.1016/j.ccell.2020.12.014); pmid: [33482121](https://pubmed.ncbi.nlm.nih.gov/33482121/)
59. A. Quintanal-Villalonga *et al.*, Multiomic analysis of lung tumors defines pathways activated in neuroendocrine transformation. *Cancer Discov.* **11**, 3028–3047 (2021). doi: [10.1158/2159-8290.CD-20-1863](https://doi.org/10.1158/2159-8290.CD-20-1863); pmid: [34155000](https://pubmed.ncbi.nlm.nih.gov/34155000/)
60. S. Sivakumar *et al.*, Integrative Analysis of a Large Real-World Cohort of Small Cell Lung Cancer Identifies Distinct Genetic Subtypes and Insights into Histologic Transformation. *Cancer Discov.* **13**, 1572–1591 (2023). doi: [10.1158/2159-8290.CD-22-0620](https://doi.org/10.1158/2159-8290.CD-22-0620); pmid: [37062002](https://pubmed.ncbi.nlm.nih.gov/37062002/)
61. S. Sivakumar *et al.*, Integrative analysis of a large real-world cohort of small cell lung cancer identifies distinct genetic subtypes and insights into histological transformation. *Cancer Discov.* **13**, 1572–1591 (2023). doi: [10.1158/2159-8290.CD-22-0620](https://doi.org/10.1158/2159-8290.CD-22-0620); pmid: [37062002](https://pubmed.ncbi.nlm.nih.gov/37062002/)
62. J. W. Park *et al.*, Reprogramming normal human epithelial tissues to a common, lethal neuroendocrine cancer lineage. *Science* **362**, 91–95 (2018). doi: [10.1126/science.aat5749](https://doi.org/10.1126/science.aat5749); pmid: [30287662](https://pubmed.ncbi.nlm.nih.gov/30287662/)
63. D. T. Montoro *et al.*, A revised airway epithelial hierarchy includes CFTR-expressing ionocytes. *Nature* **560**, 319–324 (2018). doi: [10.1038/s41586-018-0393-7](https://doi.org/10.1038/s41586-018-0393-7); pmid: [30069044](https://pubmed.ncbi.nlm.nih.gov/30069044/)
64. H. Mou *et al.*, Airway basal stem cells generate distinct subpopulations of PNECs. *Cell Rep.* **35**, 109011 (2021). doi: [10.1016/j.celrep.2021.109011](https://doi.org/10.1016/j.celrep.2021.109011); pmid: [33882306](https://pubmed.ncbi.nlm.nih.gov/33882306/)
65. M. Shivaraju *et al.*, Airway stem cells sense hypoxia and differentiate into protective solitary neuroendocrine cells. *Science* **371**, 52–57 (2021). doi: [10.1126/science.aba0629](https://doi.org/10.1126/science.aba0629); pmid: [33384370](https://pubmed.ncbi.nlm.nih.gov/33384370/)
66. A. E. Vaughan *et al.*, Lineage-negative progenitors mobilize to regenerate lung epithelium after major injury. *Nature* **517**, 621–625 (2015). doi: [10.1038/nature14112](https://doi.org/10.1038/nature14112); pmid: [25533958](https://pubmed.ncbi.nlm.nih.gov/25533958/)
67. M. E. Beaulieu *et al.*, Intrinsic cell-penetrating activity propels Omomyc from proof of concept to viable anti-MYC therapy. *Sci. Transl. Med.* **11**, eaar5012 (2019). doi: [10.1126/scitranslmed.aar5012](https://doi.org/10.1126/scitranslmed.aar5012); pmid: [30894502](https://pubmed.ncbi.nlm.nih.gov/30894502/)
68. T. E. Speltz *et al.*, Targeting MYC with modular synthetic transcriptional repressors derived from bHLH DNA-binding domains. *Nat. Biotechnol.* **41**, 541–551 (2023). doi: [10.1038/s41587-022-01504-x](https://doi.org/10.1038/s41587-022-01504-x); pmid: [36302987](https://pubmed.ncbi.nlm.nih.gov/36302987/)
69. M. C. Basil *et al.*, Human distal airways contain a multipotent secretory cell that can regenerate alveoli. *Nature* **604**, 120–126 (2022). doi: [10.1038/s41586-022-04552-0](https://doi.org/10.1038/s41586-022-04552-0); pmid: [35355013](https://pubmed.ncbi.nlm.nih.gov/35355013/)
70. P. Kadur Lakshminarasimha Murthy *et al.*, Human distal lung maps and lineage hierarchies reveal a bipotent progenitor. *Nature* **604**, 111–119 (2022). doi: [10.1038/s41586-022-04541-3](https://doi.org/10.1038/s41586-022-04541-3); pmid: [35355018](https://pubmed.ncbi.nlm.nih.gov/35355018/)
71. W. Hill *et al.*, Lung adenocarcinoma promotion by air pollutants. *Nature* **616**, 159–167 (2023). doi: [10.1038/s41586-023-05874-3](https://doi.org/10.1038/s41586-023-05874-3); pmid: [37020004](https://pubmed.ncbi.nlm.nih.gov/37020004/)
72. C. Mascoux *et al.*, Immune evasion before tumour invasion in early lung squamous carcinogenesis. *Nature* **571**, 570–575 (2019). doi: [10.1038/s41586-019-1330-0](https://doi.org/10.1038/s41586-019-1330-0); pmid: [31243362](https://pubmed.ncbi.nlm.nih.gov/31243362/)
73. C. Martinez-Ruiz *et al.*, Genomic-transcriptomic evolution in lung cancer and metastasis. *Nature* **616**, 543–552 (2023). doi: [10.1038/s41586-023-05706-4](https://doi.org/10.1038/s41586-023-05706-4); pmid: [37046093](https://pubmed.ncbi.nlm.nih.gov/37046093/)
74. P. Selenica *et al.*, APOBEC mutagenesis, kataegis, chromothripsis in EGFR-mutant osimertinib-resistant lung adenocarcinomas. *Ann. Oncol.* **33**, 1284–1295 (2022). doi: [10.1016/j.annonc.2022.09.151](https://doi.org/10.1016/j.annonc.2022.09.151); pmid: [36089134](https://pubmed.ncbi.nlm.nih.gov/36089134/)
75. R. Buisson *et al.*, Passenger hotspot mutations in cancer driven by APOBEC3A and mesoscale genomic features. *Science* **364**, eaaw2872 (2019). doi: [10.1126/science.aaw2872](https://doi.org/10.1126/science.aaw2872); pmid: [31249028](https://pubmed.ncbi.nlm.nih.gov/31249028/)
76. S. Henderson, A. Chakravarthy, X. Su, C. Boshoff, T. R. Fenton, APOBEC-mediated cytosine deamination links PIK3CA helical domain mutations to human papillomavirus-driven tumor development. *Cell Rep.* **7**, 1833–1841 (2014). doi: [10.1016/j.celrep.2014.05.012](https://doi.org/10.1016/j.celrep.2014.05.012); pmid: [24910434](https://pubmed.ncbi.nlm.nih.gov/24910434/)

ACKNOWLEDGMENTS

Funding: This work was supported by the National Cancer Institute (NCI) NIH cooperative agreement U01CA224326 (to H.V.); NCI NIH grants P01CA120964 and R35CA197588 (to L.C.C.); NCI NIH grants R01CA256188, R01CA280414, R01CA280572, and R21CA266660-01 (to A.M.L.); the Burroughs Wellcome Fund (to A.M.L.); the Lung Cancer Research Foundation (to A.M.L.); the Damon Runyon Cancer Research Foundation fellowship DRG-2343-18 (to E.E.G.); and NIH training grant T32 GM132083 (to E.M.E.). The Varmus lab is supported in part by the Lewis Thomas University Professor endowment. **Author contributions:** Conceptualization: E.E.G. and H.V. Methodology: E.E.G., E.M.E., M.J.H., K.L., J.T., B.D.S., L.C.C., and A.M.L. Experimental Design: E.E.G., E.M.E., A.M.L., and H.V. Visualization: E.E.G., E.M.E., M.J.H., and A.M.L. Funding acquisition: E.E.G., L.C.C., A.M.L., and H.V. Supervision: H.V. and A.M.L. Pathology review: C.Z. Writing – original draft: E.E.G.

Writing – review and editing: all authors. **Competing interests:** L.C.C. is a cofounder and member of the Scientific Advisory Board (SAB) and holds equity in Faeth Therapeutics, Volastra Therapeutics, and Larkspur Therapeutics. He is also a cofounder, former member of the SAB and holds equity in Agios Pharmaceuticals and Petra Pharmaceuticals (now owned by Loxo/Lilly). These companies are developing novel therapies for cancer. L.C.C.'s laboratory has previously received some financial support from Petra Pharmaceuticals. None of these companies are currently providing support for the Cantley laboratory. H.V. is a member of the SABs of Volastra, Dragonfly Therapeutics, and Surrozen. None of these companies are currently providing support for the Varmus laboratory. All other authors declare no competing interests. **Data and materials availability:** Lead contact: Requests for resources should be directed to and will be fulfilled by Eric E. Gardner (eeg2001@med.cornell.edu) or Ashley M. Laughney (asl4003@med.cornell.edu). Materials: All mouse models, organoids derived from mice, and plasmids described in this work will be made available to investigators through an institutional or third-party Material Transfer Agreement (MTA) upon reasonable request. Select plasmids will be submitted to Addgene upon manuscript acceptance. Not all mouse strains are currently active in the Varmus Laboratory colony—please contact Eric E. Gardner for specific information and availability. Data and code: The processed single-cell data and relevant code, including Docker environments with Jupyter notebooks demonstrating key analyses, are available on either the Gene Expression Omnibus (GEO no. GSE248207) or Laughney Lab GitHub (https://github.com/LaughneyLab/Lung_Histological_Transformation). **License information:** Copyright © 2024 the authors, some rights reserved; exclusive licensee American Association for the Advancement of Science. No claim to original US government works. <https://www.science.org/about/science-licenses-journal-article-reuse>

SUPPLEMENTARY MATERIALS

[science.org/doi/10.1126/science.adj1415](https://doi.org/10.1126/science.adj1415)

Materials and Methods

Supplementary Text

Figs. S1 to S15

Tables S1 to S4

References (77–115)

MDAR Reproducibility Checklist

Submitted 23 June 2023; accepted 8 December 2023

10.1126/science.adj1415